# Detection of x-rays by a surface acoustic delay line in contact with a diamond crystal

Dimitrios Topaltzikis,[1, a)] Marek Wielunski,[1] Andreas L. Hoerner,[2] Matthias Kuess,[2] Alexander Reiner,[2] Theodor Grünwald,[2] Matthias Schreck,[2] Achim Wixforth,[2] and Werner Rühm[1]

[1)] *Helmholtz Zentrum München German Research Center for Environmental Health, Ingolstädter Landstr. 1, 85764 Neuherberg, Germany*

[2)] *Institut für Physik, Universität Augsburg, D-86135 Augsburg, Germany*

(Dated: 3 March 2021)

In this study, we present proof-of-concept for an x-ray detector. The hybrid device consists of a synthetic single crystal diamond in mechanical contact with a piezoelectric lithium niobate ($LiNbO_3$) surface acoustic wave (SAW) delay line. Upon x-ray irradiation, the diamond crystal experiences a change in conductivity which in turn is very sensitively influencing the SAW transmission on the delay line. This change in SAW attenuation is directly used to monitor the x-ray beam intensity. The SAW attenuation shows a monotonic variation with dose rate $D$ in the studied range between 100 and 1800 G/s. While the response time leaves room for further improvement, the SAW detection principle offers the unique possibility for wireless remote powering and sensing.

Detection of x-rays has been the subject of continuous research since their discovery by W. C. Röntgen in 1895. The extensive use of x-rays for research, in industry and medicine, has prompted the development of detectors needed for absolute intensity measurements as well as for the protection of personnel and public health.[1] Various solutions have been developed to cope with the broad range of energies and dose rates typically used in the different applications. According to the basic detection mechanism, they can be classified into the following categories:[2] x-ray films, phosphor- or scintillator-based detectors, gas detectors and semiconductor-based solid-state detectors. The latter devices are gaining increasing importance as they benefit from the unceasing improvement of semiconductor materials. Furthermore, the wide range of stopping powers and band gap energies that are characteristic for these materials offer a plethora of options with respect to the targeted applications. Semiconductor-based detectors typically exhibit a significantly higher material density than gas detectors which qualifies them specifically for dosimetric measurements of small beams with high spatial resolution. In addition, their ionization energy is mostly lower than that of gas detectors and scintillators which means higher signals.

Among the potential semiconductor materials, diamond excels in several important properties. First, the tissue equivalence of carbon (which is of high relevance for clinical dosimetry) guarantees a nearly identical particle and energy dependence of the energy deposition in diamond and human tissue thus requiring only minor correction factors. Second, competing semiconductor materials like the III-V compounds GaAs or GaN exhibit low atomic displacement energies which make them prone to strong radiation damage. In contrast, diamond's high cohesive energy ensures excellent radiation hardness thus enabling long term stable operation.[3] Third, the low mass attenuation coefficient can be of advantage when intensity and position of a beam are to be measured without undue attenuating of its intensity[4] or in the case that the low energy range of x-ray photons to be detected extends down to below 10 keV.

Since the invention of interdigital transducers (IDTs) in 1965,[5] SAW devices have found a broad range of applications in telecommunication industry as filters, oscillators or transformers.[6] Coated with specific recognition layers they can be used as chemical sensors.[7–9] Furthermore, the SAW structures offer the potential for wireless sensing.[10,11] Finally, they can be operated as actuators for the micro-manipulation of small droplets.[12]

In the field of detectors for ionizing radiation the concept has been explored for the detection of UV radiation.[13–15] Equivalent studies with higher energy photons (x- or $\gamma$-rays) are still missing from literature. Previous investigations on the operation of SAW devices in nuclear environment suggested that such devices are radiation hard and there is no permanent damage by exposure to ionizing radiation.[16]

SAW-based radiation detectors follow the operation principles of sandwich structures. The latter have been extensively used in the field of semiconductor physics to study the interaction of SAWs with the charge carriers in bulk crystals or layers. For these sandwich structures, the following relationship between the bulk conductivity $\sigma$ of the semiconductor in vicinity of the SAW delay line and the attenuation $\Gamma$ of the propagating SAW has been reported,[17]

$$\Gamma = \frac{\omega}{v_0}\frac{K^2_{\text{eff}}}{2}\frac{\frac{\omega_r}{\omega}}{1+(\frac{\omega_r}{\omega})^2} \tag{1}$$

with $\omega$ and $v_0$ the measuring frequency in the laboratory frame and the Rayleigh velocity of the SAW, respectively. Furthermore, $\omega_r = \sigma/(\varepsilon_1+\varepsilon_2)$ denotes the so-called conductivity relaxation frequency of the semiconductor under consideration, $\varepsilon_1$ and $\varepsilon_2$ are the dielectric constants of the piezoelectric substrate and the half sphere above it, respectively. $K^2_{\text{eff}}$ represents the electromechanical coupling factor of the piezoelectric material and $\omega/v_0 = k_{\text{SAW}} = 2\pi/\lambda_{\text{SAW}}$ is the wave vector of the SAW. For quasi two dimensional (i.e., thickness $d \ll \lambda_{\text{SAW}}$) conducting layers in the vicinity of the SAW delay line, a

[a)] Author to whom correspondence should be addressed:dimitrios.topaltzikis@protonmail.ch

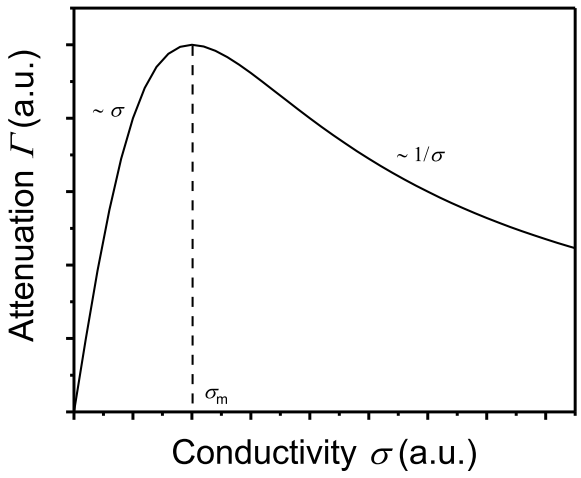


FIG. 1. Plot of Equation (2), representing the correlation between the attenuation $\Gamma$ and the conductivity $\sigma$.

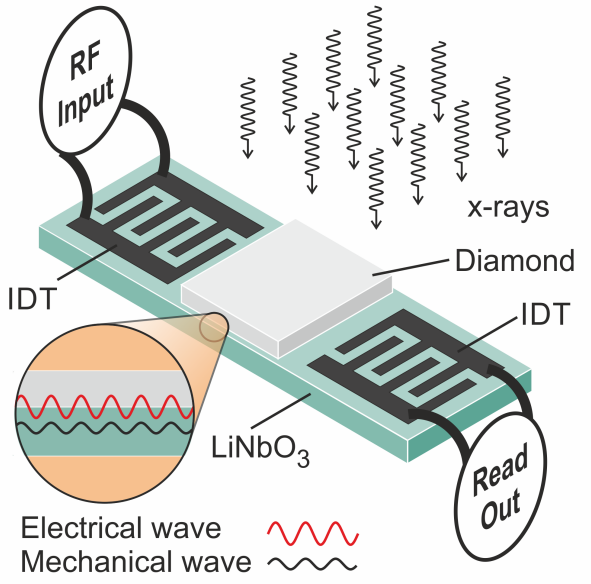


FIG. 2. Schema of the hybrid structure under irradiation with x-rays. The CVD diamond is mechanically pressed against the surface of the $LiNbO_3$ substrate. The whole structure is exposed to the photons which hit first the diamond crystal. The electric field associated with the surface acoustic wave penetrates into the diamond crystal across the very small gap.

simplified, frequency independent interaction model can be applied,[18]

$$\Gamma = \frac{\omega}{v_0}\frac{K_{\mathrm{eff}}^2}{2}\frac{\frac{\sigma}{\sigma_{\mathrm{m}}}}{1+(\frac{\sigma}{\sigma_{\mathrm{m}}})^2} \qquad (2)$$

where $\sigma_{\mathrm{m}} = v_0(\varepsilon_1 + \varepsilon_2)$ is a material dependent constant. For a measurement frequency $\omega = \text{const.}$, both equations (1) and (2) give essentially the same results, namely $\Gamma$ being proportional to $\sigma$ for low conductivities $\sigma < \sigma_{\mathrm{m}}$ and $\Gamma$ scaling proportional to $1/\sigma$ for high conductivities $\sigma > \sigma_{\mathrm{m}}$ (see Fig. 1).

Using the proximity coupling technique, the diamond crystal is brought into intimate contact with the surface of the delay-line by applying mechanical pressure, as shown in Figure 2. As the air gap between the crystal and delay-line is significantly smaller than the wavelength of the SAW, the electric field that accompanies the SAW can penetrate into the diamond and interact with the free carriers, while the SAW propagates exclusively along the $LiNbO_3$ substrate, due to the acoustic mismatch between the two components.[17–19]

Recent advancements in chemical vapor deposition (CVD) enable in the meantime the synthesis of diamond crystals that can fulfill all requirements relevant for application as radiation detectors.[20,21] In combination with the high sensitivity of SAW delay lines, this approach facilitates a different type of radiation detectors.

In this letter, we present the detection of continuous x-ray and $\gamma$-ray fields by a hybrid structure, consisting of a SAW delay-line prepared on a $LiNbO_3$ substrate and a synthetic diamond as sensing material located above the substrate (see Fig. 2). For launching SAWs, interdigital transducers were deposited on the 128° Y-cut X-propagated $LiNbO_3$ substrate by evaporating 5 nm of titanium (Ti) and 20 nm of gold (Au) employing optical lithography and a subsequent lift-off technique. The used Split-4 IDT pattern, results in a fundamental frequency of 113.00 MHz, which allows higher harmonic generation of the third, fifth and seventh SAW mode.

The diamond crystals for this study were grown heteroepitaxially on the multilayer substrate Ir/YSZ/Si(001). The whole process comprised the pulsed laser deposition (PLD) of an yttria-stabilized zirconia (YSZ) buffer layer on a 4-inch Si (001) wafer, the e-beam evaporation of an iridium film, followed by the bias enhanced nucleation (BEN) of epitaxial diamond and finally the long-time growth of a 1.3 mm thick crystal in a high-power microwave plasma chemical vapor deposition (MWPCVD) setup. The gas mixture during deposition consisted of 8 % $CH_4$ in $H_2$ without any intentional nitrogen ($N_2$) addition.[22,23]

After removal of Si substrate and buffer layers, several plates of $5 \times 5 \times 0.5\,\mathrm{mm}^3$ were prepared from the upper part of the sample with highest structural quality by laser cutting and mechanical polishing. The crystals were then heated for 15 min in air at $\approx 500\,^{\circ}\mathrm{C}$ in order to obtain an oxygen terminated surface which guarantees the absence of surface conductivity. Two of the crystals were used for the SAW experiments. One additional piece was equipped with ohmic Ti/Pt/Au contacts on both faces. Measurements at 50 V revealed a dark conductivity of several 100 nA which is at least four orders of magnitude higher than for typical high resistivity heteroepitaxial diamond samples.[24] Operation of this crystal as solid-state ionization chamber under irradiation with x-rays from a laboratory Mo-tube (50 kV, 20 mA) revealed a gain of $\approx 10^4$ at a dose rate $D$ of 77 mGy/s.

The final sandwich structure was fabricated on a 17.5 mm diameter chip carrier in a clean room environment. The central alignment of $LiNbO_3$ substrate on the chip carrier facilitated the fabrication of aluminum (Al) bonds between the con-

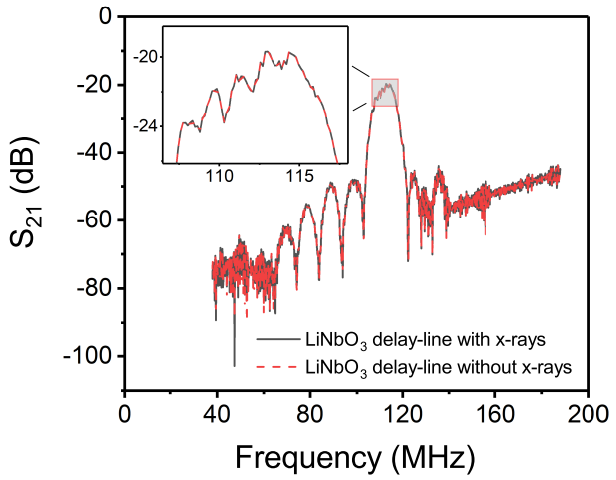


FIG. 3. Test of the $LiNbO_3$ delay-line without diamond under irradiation. Swept-frequency transmission response with and without irradiation.

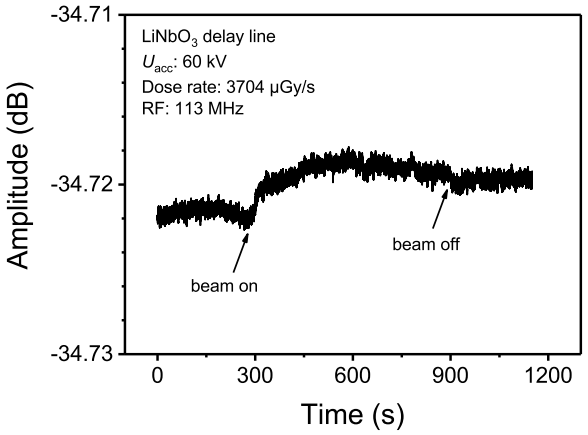


FIG. 4. Test of the $LiNbO_3$ delay-line without diamond under irradiation. Change in amplitude after switching off the x-ray beam. Throughout this study, the power of applied RF signal is -15.70 dBm using an external signal generator.

tacts of the IDTs and the Au-pins of the chip carrier. After the bonding process, the synthetic diamond sample was placed in contact with the IDTs of the SAW device using a droplet of deionized water, in order to ensure a good mechanical contact with the substrate. A modified identical chip carrier mounted with a 0.2 mm thick polystyrene plate was used to apply gentle pressure to the diamond sample. Upon completion of the fabrication procedure, the characterization of S-parameters was performed using a network analyzer, to guarantee the proper operation of the delay line.

The x-ray measurements were carried out in the IAEA/WHO Second Standard Dosimetry Laboratory (Helmholtz Zentrum München, Germany)[25] using Bremsstrahlung irradiation quality of C60 (60 kV, 45 mA) with 3.9 mm aluminum (Al) filtration. Different dose rates were realized by variation of the distance between hybrid-structure and x-ray tube. The attenuation of the used x- and $\gamma$-ray photons in diamond was low enough that one can assume a homogeneous distribution of the dose rate within the crystal. In addition, the SAW structure was also irradiated by the photon beam. A calibrated ionization chamber with an electrometer was applied to measure the dose rates. To observe the energy-source dependence for similar dose rates, additional radiation measurements were performed using a $^{137}$Cs $\gamma$-ray source, following the same experimental protocol. All radiation measurements were performed in air, under controlled temperature and humidity. The performance of the device was monitored in terms of changes in SAW signal amplitude. As the fundamental frequency of the Split-4 IDTs corresponds to 113 MHz, a signal generator was employed to supply the device with a stable RF signal of this frequency. The amplitude of the transmitted signal was analyzed by a spectrum analyzer.

In a first series of experiments, we studied the sensitivity of the plain SAW device without diamond to ionizing radiation (Fig. 3). Swept-RF frequency measurements under maximum dose rate were performed. The typical transmission function ($S_{12}$) of the SAW delay line is clearly revealed with a maximum transmission at around $f_{(\max)} = 113$ MHz. Upon irradiation of the "naked SAW device", we could neither observe a shift of the resonant frequency nor a significant attenuation of the signal. Measurements were then continued by employing a spectrum analyzer with an external signal generator (Fig. 4). Irradiating the delay line at the maximum dose rate for 600 s shows a slight increase of the amplitude by 0.002 dB when the beam was switched on but no visible response after the switch off. Thus, we conclude that the effect of radiation on the signals of the SAW structure is small enough that it doesn't query the sensor concept.

Figure 5 shows the temporal evolution of the amplitude for the complete hybrid structure, i.e. SAW plus diamond, after switching the x-ray beam (dose rate $D = 1503$ $\mu$G/s) with on/off time intervals of 600 s and 1800 s, respectively. The data permit several important conclusions: First, there is a clear response of the device yielding a signal with low noise. Second, the signal has not reached a constant level even after 1800 s which indicates high settling times. Third, several repetitions of the switching with constant duty cycle reveal a good reproducibility of the generated signals. In the measurements depicted in Figure 6, the time intervals were further increased. The constant signal after about 1 h indicates that now saturation has been reached.

The long rise and decay time constants (0.5 - 1 h) are a critical feature of the measured signals. They are similar to the values that have been found in the electrical measurements of the reference crystal equipped with metal contacts, which yields strong indications that they are caused by bulk properties rather than contacts.[26] They are also in good agreement with various former studies which consistently found a correlation between high sensitivity or high gain values and long settling times.[27–29] This behaviour was attributed to the incorporation of boron which seems to be present in nearly every CVD setup as a background contamination.[23] We conclude

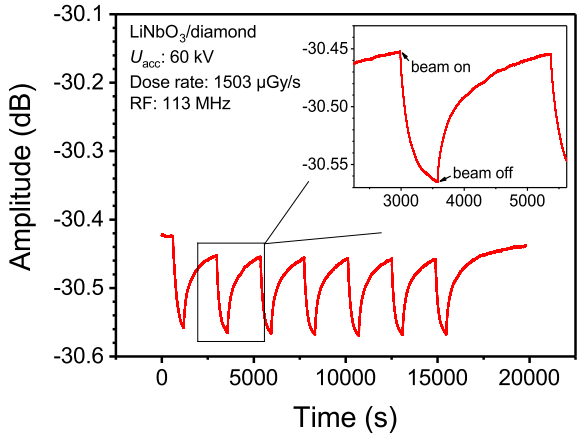


FIG. 5. Change in amplitude of the transmitted RF signal after switching of the x-ray beam that hits the SAW/diamond hybrid structure. The inset shows part of the recorded sequence. The experiment comprised sequences of 600 s exposure time and 1800 s settling time.

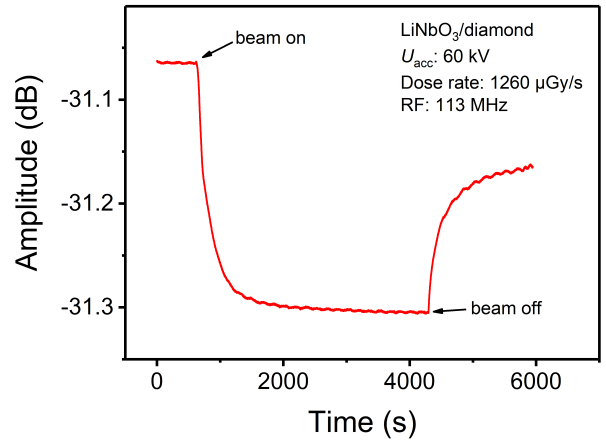


FIG. 6. Change in amplitude of the transmitted RF signal for an increased exposure time of 3600 s. Within this time interval the signal reached a saturation value. Before the experiment the device could settle without exposure overnight.

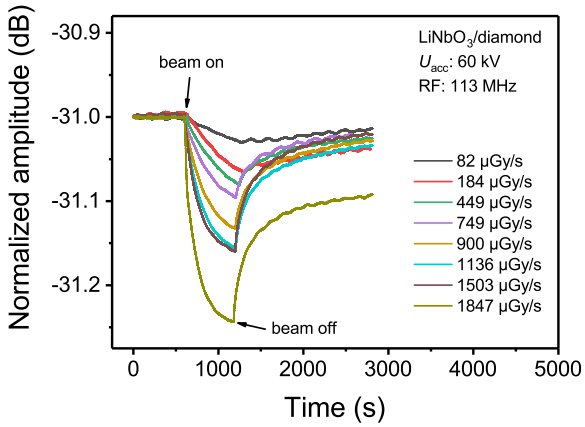


FIG. 7. Change in amplitude of the transmitted RF signal after switching x-rays with dose rates varying between 82 and 1847 $\mu$Gy/s. Before the experiment the device could settle without exposure overnight.

from the high dark conductivity that in the present crystals $[B] > [N]$, i.e. a small fraction of the boron is uncompensated by nitrogen.

The interaction relevant for the energy deposition of high energy photons in matter depends on their energy. Below $\approx 100$ keV the absorption by the photoelectric effect dominates. At higher energies Compton scattering and pair production play a major role. Relevant for the present experiment is the generation of electron hole pairs in the crystal which change its conductivity (radiation induced conductivity RIC).[30] In diamond, the energy required for creation of one e-h pair is 13 eV.[31]

In a final experiment, we explored the dose rate dependence of our device. According to the Fowler relation[30] $\sigma \propto D^{\Delta}$, the conductivity increases with dose rate $D$ while $\Delta$ typically varies between 0.5 and 1. The value of the exponent depends on the dominating recombination mechanism in the material. In commercially available diamond detectors $\Delta$ is close to 1.[32] Figure 7 shows the change in amplitude of the transmitted RF signal after switching an x-ray beam with $D$ varying between 82 and 1847 $\mu$Gy/s. In addition to the x-rays, three data points were taken under irradiation by $^{137}$Cs $\gamma$-rays ($E \approx 660$ keV). Figure 8 compares the signals for similar dose rates under x-ray and $^{137}$Cs $\gamma$-ray exposure, respectively.

For the derivation of absolute values we were faced with a general problem encountered with diamond detectors: an appreciable density of deep traps in the wide bandgap of the available crystals makes it difficult to transform the diamond sensor into an equilibrium state in acceptable time. Reports describe that the most reproducible detector results are obtained by performing several switching cycles or by pre-irradiating (priming) the sensor. The latter is even a mandatory procedure for commercial detectors containing carefully selected crystals as regularly used in hospitals.[20,32] The problem is particularly present for the high gain heteroepitaxial diamond in our experiments. For the derivation of the values shown in Figure 9, we therefore determined the difference between the amplitude measured at the end of the first exposure cycle and the end of the first recovery cycle.

Over the whole range the attenuation shows a sublinear variation with dose rate. This may partially be attributed to the relationship given by eq. (2) that predicts approximately a linear behavior at low conductivity $\sigma$ reaching a maximum and a transition to a decay $\propto 1/\sigma$ at high $\sigma$ values. In addition, nonlinearities in scaling of the carrier density and conductivity in the diamond crystal with the dose rate may also have an influence. Currently, we cannot decompose the contributions of both effects. Provided that the effects are stable and reproducible, the nonlinearities in the characteristic curve are not an obstacle for quantitative measurements when appropriate calibration procedures are applied. As shown in Figure 9, irradiation with $\gamma$-rays of $\approx 660$ keV from $^{137}$Cs source, yields a slightly higher attenuation ($\approx 0.05$ dB). Explanation of this difference requires further experiments.

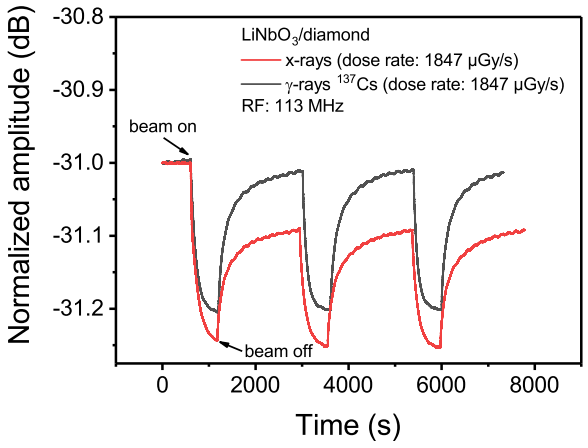


FIG. 8. Comparison of the signals generated by x-ray and $^{137}$Cs $\gamma$-ray exposure.

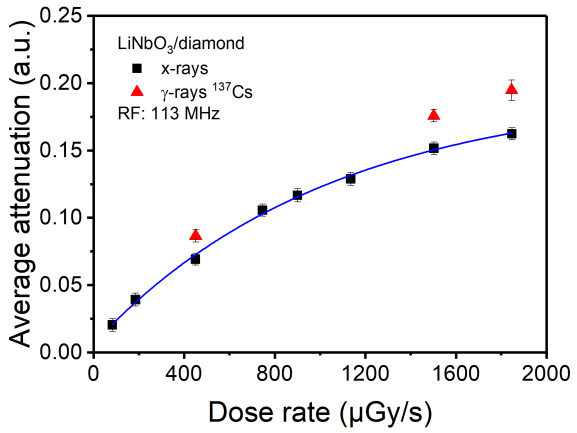


FIG. 9. Dose rate and energy dependence of the attenuation for two different excitation sources: x-rays and $^{137}$Cs $\gamma$-rays.

In conclusion, we have explored the use of a SAW delay-line in contact with a synthetic diamond crystal under illumination by ionizing radiation. It was demonstrated that radiation-induced changes of the conductivity in the diamond crystal can be detected via this hybrid structure by measuring the attenuation of the SAW signals. The long time constants for the settling of the signals after switching the irradiation is in accordance with the results of RIC measurement, which provides clear indications for bulk properties being responsible in both cases. This provides strong indications that in both cases the slow response is controlled by bulk defects without any participation of contact features.[26] Nonlinearities in the response are not considered an obstacle for technical applications since the nonlinear characteristic curves can be measured for each device by appropriate calibration procedures. Exploration of diamond crystals with lower gain is a promising route to obtain a faster response. The unique advantages of the present concept such as wireless remote powering and sensing qualify it preferably for special applications in harsh environments rather than for the substitution of standard dosimeters.

## ACKNOWLEDGMENTS

The authors would like to thank Mr. Andreas Spörhase and Mr. Adrian Mainka from Institute of Physics, University of Augsburg for the technical support and Dr. Martin Fischer for preparation of the diamond crystals. D. T. feels inclined to express gratitude to Prof. Dr. Michael J. Atkinson from Helmholtz Zentrum München for the dedicated support, as well as to Dr. John Howgate, Dr. Vedran Bandalo and Mr. Martin Schmid for their scientific help. This work was funded by Helmholtz Research School of Radiation Sciences (RS2) and by the Deutsche Forschungsgemeinschaft (DFG, German Research Foundation) - Projekt # 411398861.

## DATA AVAILABILITY

The data that support the findings of this study are available from the corresponding author upon reasonable request.

[1] J. Damodar, D. Odgers, D. Pope, and R. Hill, "A study on the suitability of the PTW microDiamond detector for kilovoltage X-ray beam dosimetry," Applied Radiation and Isotopes **135**, 104–109 (2018).
[2] Z. Luo, J. G. Moch, S. S. Johnson, and C. C. Chen, "A review on X-ray detection using nanomaterials," Current Nanoscience **13**, 364–372 (2017).
[3] K. Nordlund, S. J. Zinkle, A. E. Sand, F. Granberg, R. S. Averback, R. E. Stoller, T. Suzudo, L. Malerba, F. Banhart, W. J. Weber, *et al.*, "Primary radiation damage: A review of current understanding and models," Journal of Nuclear Materials **512**, 450–479 (2018).
[4] T. Roth, W. Freund, U. Boesenberg, G. Carini, S. Song, G. Lefeuvre, A. Goikhman, M. Fischer, M. Schreck, J. Grünert, *et al.*, "Pulse-resolved intensity measurements at a hard X-ray FEL using semi-transparent diamond detectors," Journal of synchrotron radiation **25**, 177–188 (2018).
[5] R. M. White and F. W. Voltmer, "Direct piezoelectric coupling to surface elastic waves," Applied physics letters **7**, 314–316 (1965).
[6] R. Weigel, D. P. Morgan, J. M. Owens, A. Ballato, K. M. Lakin, K. Y. Hashimoto, and C. C. Ruppel, "Microwave acoustic materials, devices, and applications," IEEE Transactions on microwave theory and techniques **50**, 738–749 (2002).
[7] A. Mujahid and F. L. Dickert, "Surface acoustic wave (SAW) for chemical sensing applications of recognition layers," Sensors **17**, 2716 (2017).
[8] I. Voiculescu and A. N. Nordin, "Acoustic wave based MEMS devices for biosensing applications," Biosensors and Bioelectronics **33**, 1–9 (2012).
[9] D. B. Go, M. Z. Atashbar, Z. Ramshani, and H.-C. Chang, "Surface acoustic wave devices for chemical sensing and microfluidics: a review and perspective," Analytical methods **9**, 4112–4134 (2017).
[10] W. C. Wilson and G. M. Atkinson, "Passive wireless sensor applications for NASA's extreme aeronautical environments," IEEE Sensors Journal **14**, 3745–3753 (2014).
[11] K. B. Pfeifer and A. N. Rumpf, "Wireless passive temperature sensor," (2012).
[12] A. Wixforth, C. Strobl, C. Gauer, A. Toegl, J. Scriba, and Z. v. Guttenberg, "Acoustic manipulation of small droplets," Analytical and bioanalytical chemistry **379**, 982–991 (2004).
[13] D. Ciplys, R. Rimeika, M. Shur, S. Rumyantsev, R. Gaska, A. Sereika, J. Yang, and M. A. Khan, "Visible–blind photoresponse of GaN-based surface acoustic wave oscillator," Applied Physics Letters **80**, 2020–2022 (2002).
[14] V. S. Chivukula, D. Ciplys, R. Rimeika, M. S. Shur, J. Yang, and R. Gaska, "Impact of photocapacitance on phase response of GaN/Sapphire SAW UV sensor," IEEE Sensors Journal **10**, 883–887 (2010).

[15] Y. Zhang, Y. Cai, J. Zhou, Y. Xie, Q. Xu, Y. Zou, S. Guo, H. Xu, C. Sun, and S. Liu, "Surface acoustic wave-based ultraviolet photodetectors: a review," Science Bulletin **65**, 587–600 (2020).

[16] N. Berg and J. Speulstra, "The operation of acoustic surface wave delay lines in a nuclear environment," IEEE Transactions on Nuclear Science **20**, 137–143 (1973).

[17] A. Wixforth, J. Scriba, M. Wassermeier, J. P. Kotthaus, G. Weimann, and W. Schlapp, "Surface acoustic waves on GaAs/$Al_xGa_{1-x}As$ heterostructures," Phys Rev B **40**, 7874–7887 (1989).

[18] A. Wixforth, J. Scriba, M. Wassermeier, J. P. Kotthaus, G. Weimann, and W. Schlapp, "Interaction of surface acoustic waves with a two-dimensional electron system in a $LiNbO_3$-GaAs/AlGaAs sandwich structure," Journal of applied physics **64**, 2213–2215 (1988).

[19] M. Rotter, A. Wixforth, J. P. Kotthaus, W. Ruile, D. Bernklau, and H. Riechert, "Quasi-monolithic GaAs/$LiNbO_3$-hybrids for acoustoelectric applications," in *1997 IEEE Ultrasonics Symposium Proceedings.*, Vol. 1 (IEEE, 1997) pp. 201–204.

[20] F. Marsolat, D. Tromson, N. Tranchant, M. Pomorski, D. Lazaro-Ponthus, C. Bassinet, C. Huet, S. Derreumaux, M. Chea, G. Boisserie, *et al.*, "Diamond dosimeter for small beam stereotactic radiotherapy," Diamond and Related Materials **33**, 63–70 (2013).

[21] C. J. H. Wort and R. S. Balmer, "Diamond as an electronic material," Materials today **11**, 22–28 (2008).

[22] S. Gsell, T. Bauer, J. Goldfuß, M. Schreck, and B. Stritzker, "A route to diamond wafers by epitaxial deposition on silicon via iridium/yttria-stabilized zirconia buffer layers," Applied Physics Letters **84**, 4541–4543 (2004).

[23] M. Schreck, P. Ščajev, M. Träger, M. Mayr, T. Grünwald, M. Fischer, and S. Gsell, "Charge carrier trapping by dislocations in single crystal diamond," Journal of Applied Physics **127**, 125102 (2020).

[24] E. Berdermann, K. Afanaciev, M. Ciobanu, M. Fischer, S. Gsell, M. Kiš, S. Lagomarsino, W. Lohmann, M. Mayr, M. Pomorski, *et al.*, "Progress in detector properties of heteroepitaxial diamond grown by chemical vapor deposition on Ir/YSZ/Si (001) wafers," Diamond and Related Materials **97**, 107420 (2019).

[25] HMGU, "Secondary Standard Dosimetry Laboratory (SSDL)," (2021).

[26] R. Di Benedetto, M. Marinelli, G. Messina, E. Milani, E. Pace, A. Paoletti, A. Pini, S. Santangelo, S. Scuderi, A. Tucciarone, *et al.*, "Influence of metal-diamond interfaces on the response of UV photoconductors," Diamond and related materials **10**, 698–705 (2001).

[27] Z. Remes, R. Petersen, K. Haenen, M. Nesladek, and M. D'Olieslaeger, "Mechanism of photoconductivity in intrinsic epitaxial CVD diamond studied by photocurrent spectroscopy and photocurrent decay measurements," Diamond and related materials **14**, 556–560 (2005).

[28] A. Secroun, A. Tallaire, J. Achard, G. Civrac, H. Schneider, and A. Gicquel, "Photoconductive properties of lightly N-doped single crystal CVD diamond films," Diamond and related materials **16**, 953–957 (2007).

[29] M. Liao, Y. Koide, J. Alvarez, M. Imura, and J.-P. Kleider, "Persistent positive and transient absolute negative photoconductivity observed in diamond photodetectors," Physical Review B **78**, 045112 (2008).

[30] J. F. Fowler, "Radiation-induced conductivity in the solid state, and some applications," Physics in Medicine & Biology **3**, 395 (1959).

[31] H. Pernegger, "High Mobility Diamonds and Particle Detectors," in *Physics and Applications of CVD Diamond* (John Wiley & Sons, Ltd, 2008) Chap. 12, pp. 309–328, https://onlinelibrary.wiley.com/doi/pdf/10.1002/9783527623174.ch12.

[32] P. W. Hoban, M. Heydarian, W. A. Beckham, and A. H. Beddoe, "Dose rate dependence of a PTW diamond detector in the dosimetry of a 6 MV photon beam," Physics in Medicine & Biology **39**, 1219 (1994).